Lumen Border Detection of Intravascular Ultrasound via Denoising of Directional Wavelet Representations

Amin Katouzian[3], Elsa Angelini[1], Auranuch Lorsakul[3], Bernhard Sturm[2], and Andrew F. Laine[3,4]

[1] Institut TELECOM, TELECOM ParisTech, CNRS LTCI, Paris, France
[2] Volcano Corporation, Rancho Cordova, CA USA
[3] Biomedical Engineering and
[4] Radiology Departments, Columbia University, New York, NY USA
Laine@columbia.edu

Abstract. In this paper, intravascular ultrasound (IVUS) grayscale images, acquired with a single-element mechanically rotating transducer, are processed with wavelet denoising and region-based segmentation to extract various layers of lumen contours and plaques. First, IVUS volumetric data is expanded on complex exponential multi-resolution basis functions, also known as Brushlets, which are well localized in the time and frequency domains. Brushlet denoising has previously demonstrated a great aptitude for denoising ultrasound data and removal of blood speckle. A region-based segmentation framework is then applied for detection of lumen border layers, which remains a challenging problem in IVUS image analysis for images acquired with a single element, mechanically rotating 45 MHz transducer. We evaluated a hard thresholding operator for Brushlet denoising, and compared segmentation results to manually traced lumen borders. We observed good agreement and suggest that the proposed algorithm has a potential to be used as a reliable pre-processing step for accurate lumen border detection.

Keywords: Brushlet, Intravascular Ultrasound (IVUS), Denoising, Border Detection, Lumen, Thresholding.

1 Introduction

Cardiovascular disease (CVD) remains the leading cause of death worldwide. In 2004, CVD took about 800,000 lives in the United States with more than half of them due to atherosclerotic plaques [1]. There has been extensive interest in developing new imaging modalities to screen the progression and regression of atherosclerotic plaques in the past decade. Among them, intravascular ultrasound (IVUS) is the most widely used, real-time, and inexpensive imaging modality that not only provides pathological as well as morphological cross-sectional grayscale images of arterial walls but also makes atherosclerotic tissue characterization feasible, using IVUS

N. Ayache, H. Delingette, and M. Sermesant (Eds.): FIMH 2009, LNCS 5528, pp. 104–113, 2009.

radiofrequency (RF) signals and images [2,3]. IVUS image segmentation has been a subject of interest for researchers due to the rapidly growing use of this imaging modality in catheterization procedures for the following two reasons. First, one important parameter during angioplasty or stent implantation procedure, is the ratio of lumen to vessel wall cross sectional area for regions of stenosis. For instance, the interventional cardiologist uses these measurements to select the appropriate type, length and diameter of a stent. Secondly, vessel walls and lumen contours are required to be traced prior to tissue characterization and plaque RF signal extraction. Pullback IVUS data files contain hundreds of cross-sectional images. The automatic extraction of vessel wall and lumen borders in those images has been the topic of various research efforts [4,5,6,7] and remains a challenging image processing problem.

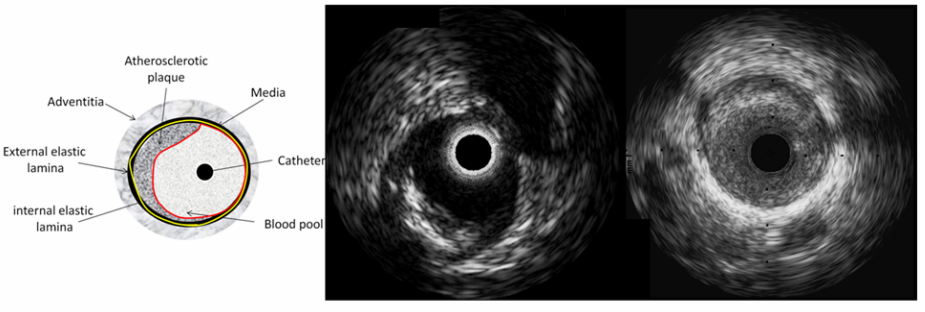

Fig. 1. Schematic cross-sectional anatomy of arterial wall and atherosclerotic plaque, the lumen border (red) and vessel wall border (yellow) (a), two distinct cross-sectional grayscale IVUS images acquired with 64-elements phased-array 20MHz (b) and single-element rotating 45MHz (c) VOLCANO transducers

Clinical application of automated segmentation methods has seen limited success due to the presence of the guide wire shadow, the arc of calcified plaques, catheter motion, cardiac motion, and the appearances of sub branches. In general, detection of the external vessel wall border is relatively easier than the internal lumen border. With IVUS ultrasound probes, the lumen border is better depicted in images acquired with a 64-element phased-array operating at 20 MHz transducer in comparison with those acquired with a single element mechanically rotating 45 MHz transducer. At higher center frequencies, the spatial resolution is improved at the cost of more scattering from red blood cells inside the lumen. Figure 1 illustrates the schematic cross-sectional anatomy of an arterial wall and atherosclerotic plaque along with two distinct cross-sectional grayscale IVUS images acquired with a 64-element 20MHz EagleEye Gold phased-array transducer (Volcano Corporation, Rancho Cordova, CA) as well as a single-element rotating 45MHz Revolution transducer (Volcano Corporation, Rancho Cordova, CA).

To improve image quality within a simple segmentation framework, we developped a three-dimensional (3D) Brushlet-based algorithm, taking into account blood flow during the pullback. The appearance of regions corresponding to plaques, vessel wall and surrounding fat is more stable within successive frames than the blood pool. Based on this observation, expansion using a brushlet basis followed by selective thresholding of brushlet coefficients was used to characterize persistent textures along the pull back dimension and remove random blood scattering and speckle. Denoising was performed in polar representation and results displayed in traditional Cartesian coordinates.

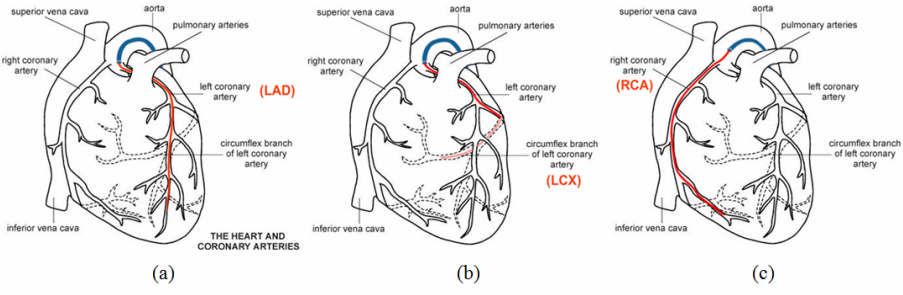

Fig. 2. The heart and coronary arteries. Schematic illustration of advanced catheter (red) into LAD (a) LCX (b) and RCA (c).

The segmentation of denoised images was then performed with region-based partitioning, Markovian regularization, and an iterated conditional mode (ICM) classification algorithm [8], based on 4 classes. Extraction of the different layers, corresponding to the ICM-classes, was finalized with a parametric deformable model.

This paper is organized as follows. Section 2 describes the acquisition system specification and data collection methodology. We then review brushlet analysis, denoising and segmentation algorithms in Section 3. The experimental results are then demonstrated in Section 4. The paper is summarized with conclusions in Section 5.

2 Data Collection

We collected IVUS grayscale images from three patients using a single element mechanically rotating 45 MHz Revolution™ transducer and s5™ imaging system manufactured by Volcano Corporation (Rancho Cordova, CA). The catheter was advanced on top of the guide wire from the femoral artery toward the site of coronary arterial occlusion (i.e. right coronary artery (RCA), left anterior descending (LAD), left circumflex (LCX)) via the aorta. Figure 2 illustrates schematically the heart, coronary arteries and the catheter path. During image acquisition, the catheter is pulled back from the distal to proximal locations with a speed of 0.5mm/sec,

acquiring 30 frames/sec. Ultimately, each grayscale IVUS frame was constructed from 256 radial lines spanning 360^{o} and 360 samples/line after decimation and interpolation in radial and lateral directions, respectively. The original images, acquired in polar coordinates, were then mapped to Cartesian coordinates to construct typical IVUS images, as shown in Figure 3.

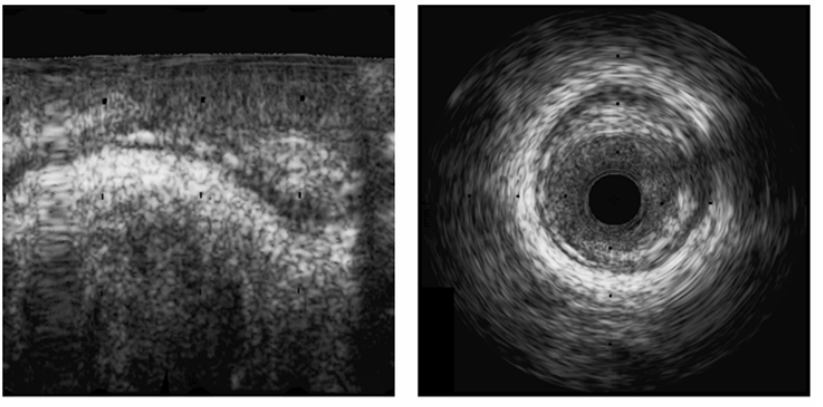

Fig. 3. Grayscale IVUS image in polar (a) and Cartesian (b) domains

3 Methodology

We applied a 3D (cross-sectional image of arterial content + pull-back distance) overcomplete brushlet analysis to sub-blocks of IVUS frames in polar coordinates during each pullback. We assumed a strong spatial coherence in the appearance of plaque, arterial wall and surrounding fat within the analysis blocks. This coherence is organized in concentric circular layers and is better expressed and visualized in polar representations of the image data. Also, brushlet tiling and expansion is based on a regular square lattice which is best correlated with homogeneous textured patterns in polar (r,θ) rather than Cartesian (x,y) image representation. The presence of blood speckle within the volume of analysis is also considered to be dynamic due to blood flow. The underlying hypothesis for brushlet denoising, is that blood speckle can be removed by including the pull-back dimension in the analysis which creates "virtual textures" in the spatial-frequency domain. Finally, the results are mapped back to Cartesian coordinates for visual display.

3.1 Brushlet Basis

Brushlets are windowed complex exponential functions in the family of steerable wavelets and were introduced in [9]. They divide the real axis into subintervals $[a_n, a_{n+1}]$ of length l_n, and define a brushlet analysis function as follows

$$u_{j,n}(x) = b_n\left(x - {l_n}/{2}\right)e_{j,n}(x) + v(x-a_n)e_{j,n}(2a_n - x) - v(x-a_{n+1})e_{j,n}(2a_{n+1} - x) \quad (1)$$

The b_n and v are two windowed functions, which are defined from the ramp function. The complex orthonormal basis function $u_{j,n}$, can be constructed using these two functions along with the complex exponential function $e_{j,n}$ that is defined as $e_{j,n}(x) = \frac{1}{\sqrt{l_n}} e^{-2i\pi j\frac{(x-a_n)}{l_n}}$. Given any one-dimensional signal f in $L^2(R)$, its Fourier transform $\hat{f}$ can be projected onto the brushlet basis as $\hat{f} = \sum_n \sum_j \hat{f}_{n,j} u_{n,j}$ where $\hat{f}_{n,j}$ are the brushlet coefficients. It has been shown that the projected of $\hat{f}$ onto the brushlet basis can be implemented in an efficient fashion using a folding technique and fast Fourier transform (FFT) [10]. In the reconstruction process, the original signal can be retrieved using inverse Fourier transform and unfolding operation.

In our application, a tensor product extension was used for the volume of IVUS data frames. Consequently, such an extension would lead to the orientation selectivity in the brushlet domain, which is described next.

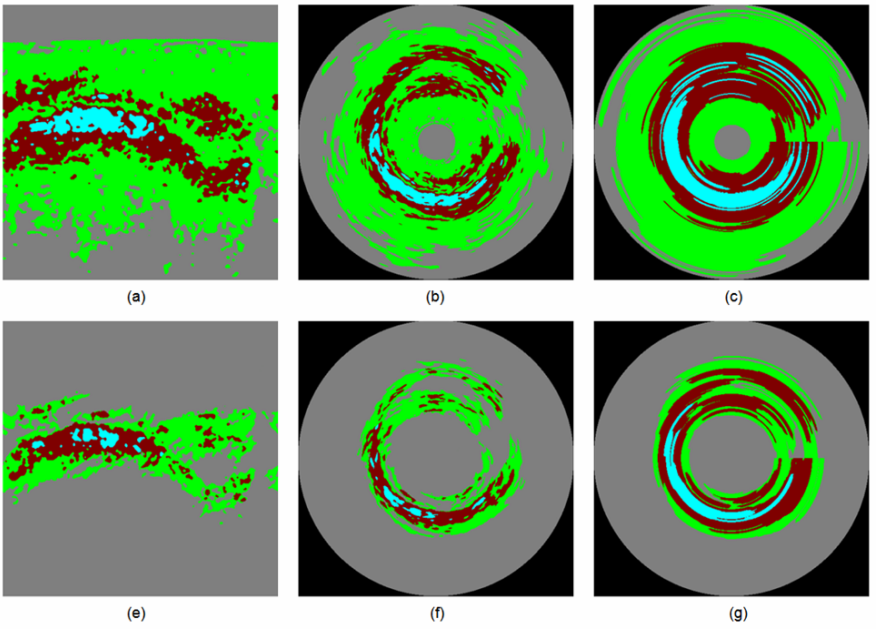

Fig. 4. ICM segmentation. 4-classes ICM results for original image in polar (a), Cartesian coordinates (b) and after dilation (c). 4-classes ICM results for denoised image in polar (d), Cartesian coordinates (e) and after dilation (f).

3.2 Frequency Tilling and Overcomplete Representation

The decomposition of the IVUS volumes onto a brushlet orthonormal basis can provide a way to capture selectable textural features of different orientations in the Fourier (brushlet) domain. Since we deal with volumetric datasets, this can be reliably performed by tilling the Fourier domain into quadrants (sub-cubes), each representing a specific size and orientation of a brushstroke, which is analogous to a wavelet scaling function.

We used an overcomplete multiscale representation of the brushlet coefficients for two reasons. First, to avoid aliasing effect and secondly, to preserve as much textural information as possible in the transform domain due to the stringent behavior of blood and plaque signals that makes the lumen border detection very challenging.

3.3 Thresholding for Removal of Blood Speckle

The purpose of this study was to offer a reliable denoising algorithm by removing blood speckle (noise), such that the resulting denoised data can be employed as an input for any 2D or 3D segmentation algorithm. We used two methods for eliminating blood noise via thresholding of the brushlet coefficients. We deployed a hard thresholding technique on real part of each brushlet coefficient.

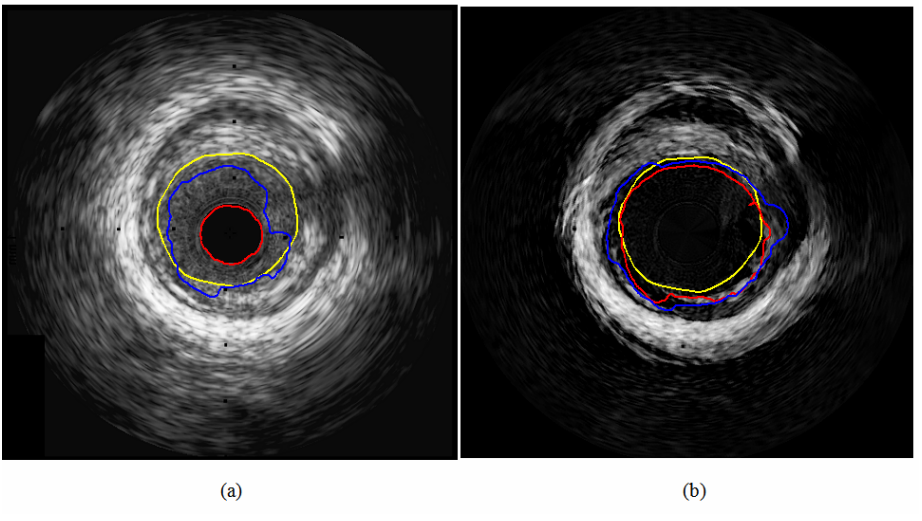

Fig. 5. Segmentation results at different layers (red, Blue) along with manually traced contour by an expert (yellow) on original (a) and denoised (b) IVUS images

3.4 Segmentation of IVUS Data

We used an iterative conditional model (ICM) segmentation framework to segment the IVUS data into 4 regions (layers), characterized by their average gray values. The

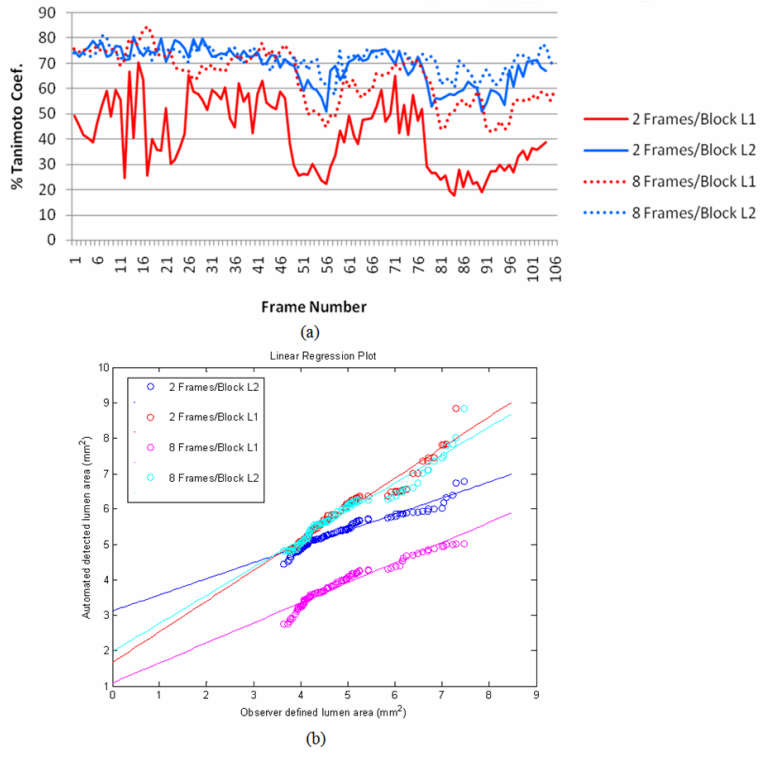

Fig. 6. Evaluation of detected contours at two layers (L1, L2) in 104 IVUS frames within a pullback with two different block sizes. Tanimoto coefficients (a), Regression analysis (b).

ICM segmentation framework corresponds to a discrete minimization of the piece-wise Mumford and Shah functional energy [11] replacing curvature constraints with a Markovian regularization of the contours. The Markovian regularization provides a very efficient computational framework to control orthogonal and vertical associations of similar class labels when applied on a regular lattice corresponding to 4-neighbor pixels in 2D. Such a constraint is ideal for circular patterns such as vessel layers, when displayed in polar coordinates. We therefore applied the ICM to the IVUS original and denoised volumes in polar coordinates. Consequently, classification results were transformed to the Cartesian coordinates for visualization and extraction of the center contours with a standard parametric deformable model applied to thresholded ICM classifications for the four classes and imposing a regular growth of vessel contour areas by iteratively initializing the deformable model at the center of the image (transducer). This extraction step was performed after dilation of the ICM classification results with a horizontal line structuring element of 70 pixels, in polar coordinates. This computational step was designed to close the open and unconnected borders to obtain better results from parametric deformable model and estimate the lumen border more precisely, as illustrated in Figure 4.

4 Results and Discussion

In the first experiment, we processed IVUS volumes of size $512\times512\times2$ and the Fourier domain was tilled using four by four by two cubes in the x, y and pull-back dimensions respectively each in an overcomplete representation. We repeated the experiment using volumes of size $512\times512\times8$ to insure adequate spatial resolution in the pull-back dimension (at an 8 slice depth). Higher spatial resolution in this dimension resulted in blurred denoised data due to the effects of the motion of the catheter and heart (without ECG gating).

Figure 5 illustrates the results of our segmentation algorithm, for the second experiment, on an original IVUS image and the resulting denoised image using a hard thresholding operator. For this purpose, the thresholding was performed in each cube empirically with the threshold value set at 50% of the maximum value of real part of the coefficients. The resulting denoised coefficients were then classified into four groups with uniform gray level values for ICM initialization. However, we only extracted the contours from the first two layers since they better approximated the true lumen border. As shown in Figure 5, the segmentation algorithm outperforms well on denoised images and the automated borders at two layers (red L1 and blue L2) are well correlated and matched with manually traced lumen border (yellow), which was traced by an expert.

Table 1. Tanimoto coefficient statistics and correlation between automated and manually traced borders in 233 frames collected from three distinct cases

	Number of Frames	***Mean Tanimoto Coefficients***	***Maximum Tanimoto Coefficients***	***Minimum Tanimoto Coefficients***	***Correlation (p<0.0001)***
Case # 1	104	$L1: 64.12 \pm 10.56$ $L2: 71.34 \pm 4.74$	$L1: 84.55$ $L2: 81.02$	$L1: 42.78$ $L2: 57.53$	$L1: 79.01$ $L2: 78.74$
Case # 2	104	$L1: 71.10 \pm 9.69$ $L2: 72.70 \pm 4.05$	$L1: 84.20$ $L2: 81.09$	$L1: 48.33$ $L2: 60.87$	$L1: 0.78$ $L2: 0.80$
Case # 3	25	$L1: 69.73 \pm 4.22$ $L2: 77.08 \pm 4.63$	$L1: 77.69$ $L2: 86.93$	$L1: 60.47$ $L2: 70.14$	$L1: 0.94$ $L2: 0.95$

For both experiments regression analysis was performed to evaluate the agreement between automated and manually traced contours for 104 frames within a pullback, Figure 6(a). In addition, we computed the Tanimoto coefficients to see how well the automated and manual contours are matched throughout the pullback, Figure 6(b). The average Tanimoto coefficients for the L1 and L2 borders were found to be 41.75 ± 13.66 and 69.16 ± 7.37, respectively in the first experiment (using block size of $512\times512\times2$) and 64.12 ± 10.56 and 71.34 ± 4.74 respectively in the second experiment (using block size of $512\times512\times8$) (case #1, Table 1). The Tanimoto coefficients measure the agreement in positioning of the automated and manually traced borders. According to Figure 6(b), the higher Tanimoto coefficients were achieved for the first 50 frames, where the pullback was more consistent (minimal motion). Our results show

that non-coherent pattern of blood speckle is better captured in longer IVUS volumes. However, the changes in plaque textures or motion artifacts become more significant and can degrade the results (as shown in frames 51 and 81, Figure 6(a)). This suggests that an adaptive processing technique might help in future efforts. Table 1 summarizes the Tanimoto coefficients statistics as well as the correlation values for 233 frames extracted from three distinct cases using block size of $512\times512\times8$ IVUS frames. Overall, the extracted contours at the second layer (L2) were found to have more agreement with corresponding manually traced borders.

5 Conclusion

In this paper we presented a new 3D denoising technique based on brushlet representations to remove blood noise in IVUS images acquired with a 45MHz single- element transducer. We further used denoised volumes as input to a 3D multi-region multi-channel segmentation algorithm to estimate the lumen border. We observed that the algorithm performs reasonably well especially so in areas of consistent pullback where there is strong spatial coherence in the appearance of plaque and minimal motion. In the future, we will try to make the thresholding adaptive, correct of motion and look at other directional informative that may provide more differentiation between blood and non-blood textures.

References

[1] American Heart Association, Heart Disease and Stroke Statistics – 2006 update, American Heart Association (2006)

[2] Nair, A., Kuban, B.D., Obuchowski, N., Vince, D.G.: Assessing spectral algorithms to predict atherosclerotic plaque composition with normalized and raw intravascular ultrasound data. Ultrasound in Med. & Biol. 27(10), 1319–1331 (2001)

[3] Katouzian, A., Baseri, B., Konofagou, E.E., Laine, A.F.: An alternative Approach to Spectrum-Based Atherosclerotic Plaque Characterization Techniques Using Intravascular Ultrasound (IVUS) Backscattered Signals. In: MICCAI-CVII 2008 (2008)

[4] Cardinal, M.H.R., Meunier, J., Soulez, G., Maurice, R.L., Therasse, E., Cloutier, G.: Intravascular Ultrasound Image Segmentation: A Three-Dimensional Fast-Marching Method Based on Gray Level Distribution. IEEE Tran. Med. Imag. 25(5), 590–601 (2006)

[5] Sonka, M., Zhang, X., Siebes, M., Bissing, M.S., DeJong, S.C., Collins, S.M., Mckay, C.R.: Segmentation of Intravascular Ultrasound Images: A Knowledge-Based Approach. IEEE Tran. Med. Imag. 14(4), 719–732 (1995)

[6] Unal, G.B., Bucher, S., Carlier, S., Slabaugh, G.G., Fang, T., Tanaka, K.: Shape-Driven Segmentation of the Arterial Wall in Intravascular Ultrasound Images. IEEE Tran. Info. Tech. Biomed. 12(3), 335–347 (2008)

[7] Klingensmith, J.D., Shekhar, R., Vince, D.G.: Evaluation of Three-Dimensional Segmentation Algorithms for the Identification of Luminal and Medial-Adventitia Borders in Intravascular Ultrasound Images. IEEE. Tran. Med. Imag. 19(10) (2000)

[8] Besag, J.: On the Statistical Analysis of Dirty Pictures. Journal of Royal Statistical Society, Series B 48(3), 259–302 (1986)

[9] Meyer, F., Coifman, R.R.: Brushlets: A tool for directional image analysis and image compression. Applied and computational harmonic analysis 4, 147–187 (1997)
[10] Ausher, P., Weiss, G., Wickerhauser, M.V.: Local sine and cosine bases of Coifman and Meyer and the construction of smooth wavelets. In: Chui, C.K. (ed.) Wavelets- A tutorial in Theory and Application. Wavelet Analysis and its Applications, vol. 2, pp. 237–256. Academic Press, San Diego (1992)
[11] Mumford, D., Shah, J.: Optimal Approximation by Piecewise Smooth Functions and Associated Variational Problems. Communication on Pure and Applied Math. 42, 544–685